

X-TIME: An in-memory engine for accelerating machine learning on tabular data with CAMs

Giacomo Pedretti, *Member, IEEE*, John Moon, Pedro Bruel, Sergey Serebryakov, Ron M. Roth, *Fellow, IEEE*, Luca Buonanno, Archit Gajjar, Tobias Ziegler, Cong Xu, Martin Foltin, Paolo Faraboschi *Fellow, IEEE*, Jim Ignowski *Senior Member, IEEE*, and Catherine E. Graves

Abstract—Structured, or tabular, data is the most common format in data science. While deep learning models have proven formidable in learning from unstructured data such as images or speech, they are less accurate than simpler approaches when learning from tabular data. In contrast, modern tree-based Machine Learning (ML) models shine in extracting relevant information from structured data. An essential requirement in data science is to reduce model inference latency in cases where, for example, models are used in a closed loop with simulation to accelerate scientific discovery. However, the hardware acceleration community has mostly focused on deep neural networks and largely ignored other forms of machine learning. Previous work has described the use of an analog content addressable memory (CAM) component for efficiently mapping random forests. In this work, we focus on an overall analog-digital architecture implementing a novel increased precision analog CAM and a programmable network on chip allowing the inference of state-of-the-art tree-based ML models, such as XGBoost, CatBoost, and others. Results evaluated in a single chip at 16nm technology show 119× higher throughput at 9740× lower latency compared with a state-of-the-art GPU, with a 19W peak power consumption.

Index Terms—In-memory computing, tree-based ML, content addressable memories

I. INTRODUCTION

EXTRACTING relevant information from structured (i.e., tabular) data is paramount in practical data science. Tabular data consist of a matrix of samples organized in rows, each of which has the same set of features in its columns, and is commonly used for medical, financial, scientific, and networking applications, enabling efficient search operations on large-scale datasets. While deep learning has shown impressive improvements in accuracy for unstructured data, such as image recognition or machine translation, tree-based machine learning (ML) models still outperform neural networks in classification and regression tasks on tabular data [1]. This difference in model accuracy is due to robustness to uninformative features of tree-based models, bias towards a smooth solution of neural networks models, and in general the need for rotation invariant models where the data is rotation invariant itself, as in the case of tabular data [1]. With high model accuracy, ease of use, and explainability [2] tree-based ML models are greatly preferred by the data science community [3], with > 74% of data scientists preferring to

use these models while < 40% choose neural networks in a recent survey.

However, tree-based models have garnered little attention in the architecture and custom accelerator research fields, particularly compared to deep learning. While small models are easily executed, performance issues for larger tree-based ML models arise due to limited inference latency both on CPU and GPUs [4], [5] originating from irregular memory accesses and thread synchronization issues. As large tree-based models are finding performance limits in existing hardware, larger models (>1M nodes) are demonstrating increasingly compelling uses in practical environments where high throughput and moderate latency are desired. For example, the winner of a recent IEEE-CIS Fraud detection competition used a tree-based ML model with 20M nodes [6]. Moreover, reducing inference latency is critical in scientific applications where for use in real-time processing, model latency must be ~100 ns [7]. Similar low latency requirements for model inference arise in a real-time in-the-loop decision, data filtering systems, or streaming data scenarios, which are common across financial, medical, and cybersecurity domains [6], [8] where tabular data and tree-based ML also dominate. Thus, these models are reaching sizes and complexity levels for meaningful real-world tasks, as they are hitting limits on inference latency and throughput in current systems. Recently, custom accelerators for tree-based ML inference have been developed based either on FPGA [7], [8] or custom ASICs [5], [9]. A common architecture in most of the accelerators mentioned above implements look-up tables (LUTs) storing the attributes of a decision tree (DT) accessed multiple times during inference, with reads based on decision paths taken during the tree traversal. Along with low latency inference, an efficient hardware representation of trees is necessary to implement the required very large models.

One promising new architectural approach for improving tree-based model inference is in-memory computing, where data are stored and processed in the same location. This approach eliminates access, transfer, and processing of data in a separate compute unit [10], reducing latency. Previous research has shown that these devices can efficiently perform multiplication functions in crossbar architectures [11]. However, crossbar architectures are limited to matrix operations, which are not useful for inference on tree-based models. Another class of in-memory computing primitives is Content Addressable Memories (CAMs) [12], [13], high-speed and highly parallel circuits that search for a given input in a table of stored words and return the matched search input's location.

G. Pedretti, J. Moon, P. Bruel, R. M. Roth, L. Buonanno, A. Gajjar, T. Ziegler, C. Xu, M. Foltin, P. Faraboschi, J. Ignowski and C.E. Graves were with the Artificial Intelligence Research Lab (AIRL), Hewlett Packard Labs, Milpitas (CA) e-mail: giacomo.pedretti@hpe.com.

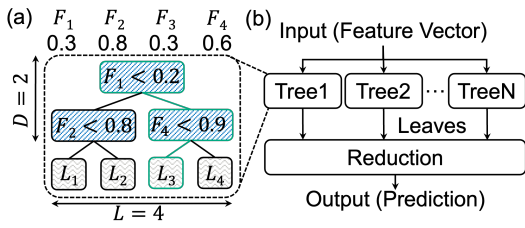


Fig. 1. Schematic illustration of (a) a decision tree and (b) a decision tree ensemble.

More recently, analog CAMs have been proposed [14] which leverage the analog states in memristor devices. An analog CAM cell performs *in situ* comparisons of stored (analog) ranges with (analog) inputs, by computing if the input is within the range. Effectively, analog CAM arrays perform a massively parallel comparison between an input vector of analog values and stored words of analog ranges. Given that DTs are a set of conditional branches, analog CAMs naturally map DTs and perform highly parallel inference of decision forests [15]. Previous work showed the potential of this approach but was limited to component-level estimation, 4-bit precision, and random forest models [15].

This work presents X-TIME, an in-memory engine for accelerating tree-based ML models with analog CAMs. In this work we demonstrate the need for a holistic architecture design, 8-bit operation, and support for multiple tree-based ML models, overcoming the limitation of previous work [15]. The major contributions of this paper compared to previous work [15] are (1) a novel analog CAM cell design and operation to perform decision tree inference at doubled (i.e. 8-bit) memristor precision (i.e. 4-bit), (2) an in-core and in-network leaf accumulation architecture to seamlessly perform inference of a large number of trees in parallel, (3) a programmable Network-on-Chip (NoC) to operate any tree-based ML model regardless of the ensemble reduction operation, (4) a compiler supporting the mapping of multiple tree-based ML models and (5) a rigorous characterization method and scaling comparison with respect to GPUs, FPGAs, and conventional digital accelerators. Our simulated evaluation shows up to $119\times$ increased throughput at $9740\times$ decreased latency in a single 19W chip.

II. BACKGROUND

A. Tree-based Machine Learning

A DT is a regression and classification ML model consisting of a set of *nodes* arranged in a tree-like structure. Each node can have multiple children nodes, but the most common case is a *binary tree*, where each node has only two children. The first node is usually called the *root*. Each node j consists of a conditional branch where a single input feature element f_i is compared with a trainable threshold T_j . The exception to this is the last node, or *leaf*, which stores the model's prediction for a given input, and which can be a class (classification) or a scalar value (regression). A balanced tree can be defined by its *depth* D , which is equal to the maximum number of nodes

in a root-to-leaf traversal. Fig. 1(a) shows an example of a DT with $L = 4$ leaves and $D = 2$.

Multiple DTs can be trained together as an ensemble for increased accuracy in classification and regression tasks. Fig. 1(b) shows a conceptual representation of a DT ensemble, where multiple trees are executed in parallel and their output combined with a *reduction* operation yields the model's final result. Examples of DT ensembles model include Random Forests (RF) [16], eXtreme Gradient Boosting (XGBoost) [17], and Categorical Boosting (CatBoost) [18]. In the case of RF, the reduction operation consists of a majority voting, while in all the others leaf values of each DT are summed.

B. Tree-based ML model inference on GPU

While training DT models is relatively fast when compared to, for example, a large deep neural network, the computations involved in inference are very irregular and not particularly suitable for CPUs and GPUs, becoming inefficient for very large models, with > 1 M nodes [6]. While CPUs can run irregular control paths fairly well, their parallelism is limited. GPUs have a very large parallelism, but suffer from the irregularity of memory access patterns, as will be explained in detail below. Recent NVIDIA libraries implementations have shown order of magnitude improvements compared to CPU and previous GPU implementations [19]. However, three different factors still limit GPU throughput and latency [4], in particular for tree ensembles. First, a high number of uncoalesced memory accesses, due to the low ratio between requested and fetched data, causes low memory efficiency. Trees are usually stored in memory with nodes from different trees interleaved in breadth-first order, resulting in coalesced memory accesses close to the root, where children nodes are more likely to be part of the same memory transaction of the parent node, but uncoalesced memory accesses further from the root. Thus, with increasing tree depth the proportion of coalesced memory accesses decreases and memory system efficiency also decreases. Second, synchronization between threads and the consequent load imbalance due to waiting for the deepest trees limits latency. A common implementation scheme on GPU assigns each tree in the ensemble to a different thread by round-robin. At the end of each thread block, a reduction operation is then performed. However, a given ensemble may contain *short* and *tall* trees, with the latter having substantially larger latency. Thus, each thread block must wait until the slowest (tallest) tree has finished processing, increasing overall latency. Finally, with a larger number of trees N_{trees} in the ensemble, the increasing number of thread blocks and the global reduction performed between thread blocks becomes a significant overhead. Multiple techniques have been proposed to increase the throughput of tree ensemble inference [4], [19], mainly by re-organizing the memory - for example, for sparse trees and scheduling of threads - but with limited impact on latency. In this work, we focus on addressing these limitations with an in-memory computing architecture using content-addressable memories.

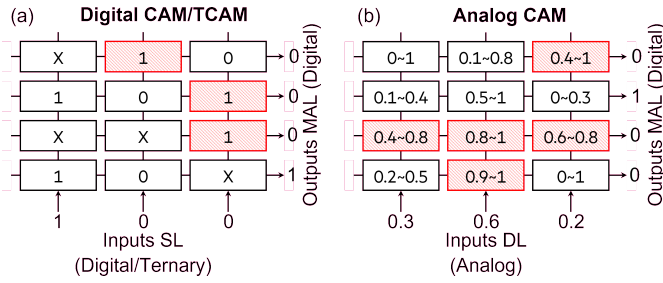


Fig. 2. Comparison of (a) a conventional CAM/TCAM and (b) an analog CAM

C. Analog Content Addressable Memory

CAMs are specialized memory devices that search a table of stored words (rows) or keys in parallel for a given input query. The CAM search output is a one-hot vector where a high value corresponds to a match between the input data query and stored row word key [12], [13]. In conventional CAMs, this output vector is converted into a single address by a priority encoder. Each CAM cell functions as both memory and bit comparison, and the input query is compared to each CAM word simultaneously to produce a high throughput, low latency few-cycle compare operation at the cost of high power and area. In addition to binary (0 and 1) values, ternary CAMs (TCAMs) have a third wildcard value, X (or “don’t care”), which can be used to compress the stored CAM table or perform partial match searches. When an X is stored or searched, that cell matches irrespective of whether the searched or stored value is 1 or 0. Fig. 2(a) shows a schematic illustration of a conventional CAM/TCAM circuit, where input queries are applied on the column search lines (SLs) and outputs are read along the row “match lines” (MALs). An XNOR operation occurs between the query values and stored cell values in the corresponding column. The MAL j th row output is produced by a bit-wise AND operation between cells along the row and returns a match (high) or mismatch (low). The red boxes in Fig. 2(a) correspond to mismatches between input and stored value. In practice, MALs are initially pre-charged high and a mismatch in a cell activates a pull-down transistor connected to MAL to discharge it, such that a match is returned only if all pull-down transistors remain off during a search operation.

TCAMs are used ubiquitously in networking applications that require high-throughput and low-latency operations, for example for packet classification and forwarding, and access control lists [12]. While offering high performance, conventional SRAM-TCAMs are power and area-hungry and require 16 transistors. Recently, there has been significant interest in developing TCAMs with memristor devices and resistive non-volatile memories [20]–[22] with compact size and low-power operation. As programming these devices is relatively slow, emerging TCAMs have targeted in-memory computing applications [13], [23] where stored value updates are infrequent.

Beyond direct digital memory operation, memristor devices have also demonstrated ranges of stable analog states of > 16 levels. Leveraging this analog state capability, recent work proposed and demonstrated an analog CAM circuit design and

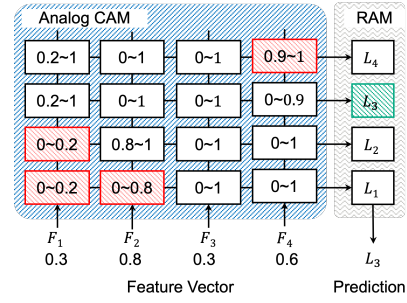


Fig. 3. DT example from Fig.1(a) with nodes mapped in an analog CAM and leaves mapped into a RAM.

operation [14] (conceptual representation in Fig 2(b)). In an analog CAM, *ranges* are stored in each cell, an analog input is applied vertically along columns and a match is returned along rows if the inputs are all within the stored range of each cell in a row. An analog CAM row implements

$$\text{MAL}_i = \bigwedge_j (T_{L,ij} \leq q_j < T_{H,ij}), \quad (1)$$

where q is the query input vector applied to DL, and T_L and T_H are the stored range thresholds for the CAM cell range lower and upper bounds, respectively. In the analog CAM circuit, no analog-to-digital conversion is required, eliminating an expensive component which is a limiting bottleneck of other analog in-memory computing primitives [24]. Multiple analog CAM circuits have been realized using different technologies such as memristor devices [14] and ferroelectric memory devices [25]. In such circuits, two analog memory elements represent the lower and upper bound thresholds. Analog CAMs have been shown to map CAM tables more efficiently [14], as well as implement novel functions, such as computing distances for memory-augmented neural networks [22], [25], decision tree inference [15] and pattern learning [26].

D. Mapping tree models to analog CAMs

The X-TIME compiler takes as input the description of a DT ensemble in a tabular mode, where each row contains the node attributes (feature ID and value) and the left/right children. The compiler traverses the tree structures extracting all the root-to-leaf paths. Finally, it maps each of them to an ACAM row. As an example, Fig. 3 shows the mapping of Fig. 1(a). Each column corresponds to a different feature of the input vector q . Each node is mapped in the column corresponding to the feature used in the node’s comparison. The comparison’s threshold value is programmed in the analog CAM’s lower and/or upper bound, according to the direction, left or right, taken by the comparison’s result for the root-to-leaf path. A “don’t care” is used if a feature is missing, by programming the full range (0 to 1 in our example) in the analog CAM cell. The feature vector (query) is applied on the DL and the output on the MAL is high for the matched branch, i.e. the traversed root-to-leaf path, in a single CAM operation. This mapping requires the number of CAM rows to match the number of tree leaves, and the number of CAM columns to match the number of features N_{feat} . MALs can be connected directly

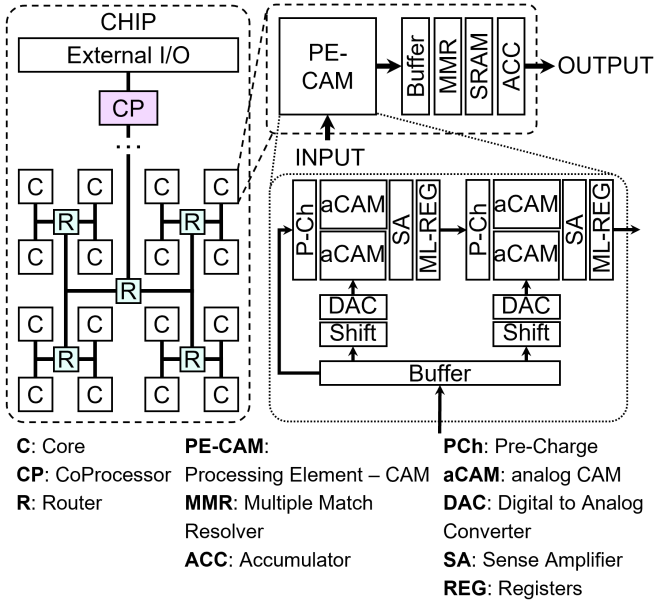


Fig. 4. Architecture hierarchy

to the Word Lines (WLs) of a conventional RAM storing leaf values to return the model’s prediction. Effectively, the analog CAM traverses root-to-leaf paths, and the RAM retrieves leaf values.

Previous results of this approach have shown significant speedups for RF inference [15] and reduced energy consumption compared to both GPU and state-of-art ASICs [27], although with limited architecture investigation for scaling and no flexibility to accommodate different dataset or model types. In this work, we present a complete architecture development and study for handling multiple DT ensemble algorithms such as RF, XGBoost, and CatBoost, and learning tasks such as regression, binary classification, and multi-class classification with the same architecture. In addition, we extend the use of the previously presented analog CAM [14], [15] circuit to support higher precision data by developing a flexible connectivity strategy and bit-arithmetic refactoring. We compare the performance of our architecture on state-of-the-art tabular dataset ML tasks against GPU, FPGA and digital ASIC, showing a large improvement in latency and throughput while using a single chip with limited power consumption.

III. ARCHITECTURE ORGANIZATION

Fig. 4 shows the internal architecture of an X-TIME single-chip accelerator. The accelerator is composed of a group of cores connected by an H-tree NoC topology converging to a co-processor (CP). Each core contains an analog CAM array acting as a processing element (PE-CAM), buffer, multiple match resolver (MMR), SRAM memory, and accumulator (ACC) (i.e. feedback adder). Typical CAM architectures also contain similar elements but the memory is used as an address encoder rather than for storing leaves [12]. To map models larger than a single array, each PE-CAM has a number of *stacked* arrays (extended row-wise) and *queued* arrays (extended column-wise) to handle more and larger words, re-

spectively. Stacked arrays share the same peripherals, namely the Pre-Charger (P-Ch), the Digital Analog Converter (DAC), the Sense Amplifier (SA), and the Match-Line Register (ML-REG). The connection of queued arrays ensures that only previously matched lines are charged by making the ML-REG of array i feed the P-Ch of the array $i + 1$.

A. Inference

X-TIME compiler maps the trained trees to the cores according to Fig. 3. Training is performed using standard libraries such as *scikit-learn* [28] or XGBoost [17]. XGBoost outputs a table with $N_{leaves} + N_{nodes}$ (where N_{leaves} is the total number of leaves in the ensemble) rows each storing the node ID, left and right child ID, node value, node feature, leaf value (if it is a leaf) and tree ID. Converting this table for CAM usage, we obtain a new table of size $L \times (2N_{feat} + 3)$ with each row storing the lower/upper bound for each feature, the leaf value, class ID/label (in the case of multi-class classification) and tree ID, representing the model ensemble for our architecture. The X-TIME compiler assigns trees to cores via round-robin, directly mapping the first $L \times (2N_{feat})$ columns of a tree to the lower and upper bound of the analog CAM circuit, and the third-last column to the SRAM. Class and tree ID are uniquely represented in the core address. The largest ensemble in our architecture is constrained by the maximum number of leaves $N_{leaves,max}$ in all trees and the number of available cores N_C . If $L < N_{words}/2$, multiple trees can be mapped to a single core, where $N_{words} = N_{stacked} \times H$ is the number of words addressable by each core (with H number of rows in an analog CAM array and $N_{stacked}$ number of arrays stacked).

During inference, a feature vector is sent through the network to a core and searched in the PE-CAM. Each queued analog CAM block receives a different portion of the feature vector which is converted into analog voltage values by a DAC. A shift operation before the conversion is performed to increase operation precision (as discussed in section III-B). A logical AND operation is inherently performed between the queued arrays, similar to MAL segmentation used in modern TCAMs to maintain high throughput where MALs are divided into sections of shorter words with an AND between individual MAL results. Connecting multiple TCAM arrays with common MALs is logically equivalent to a larger TCAM, with the bit-wise AND operation between TCAM cells on the same MAL now extended between arrays. In our case, the analog CAM stores a branch split into multiple analog CAM arrays and reconstructed by means of the logical AND, such that only if all branch nodes arranged in multiple arrays are matched will a match be returned on the corresponding MAL.

The final output of the PE-CAM is stored in a buffer and fed into the MMR which selects only one match signal to proceed logically. The MMR is needed due to the possibility of mapping multiple trees in a single core. In fact, given $N_{trees,core}$ mapped to a core, for each inference, the PE-CAM would return $N_{trees,core}$ matches in the form of a sparse Boolean vector with $N_{trees,core}$ match values (“1”s). The MMR generates $N_{trees,core}$ one-hot Boolean vectors

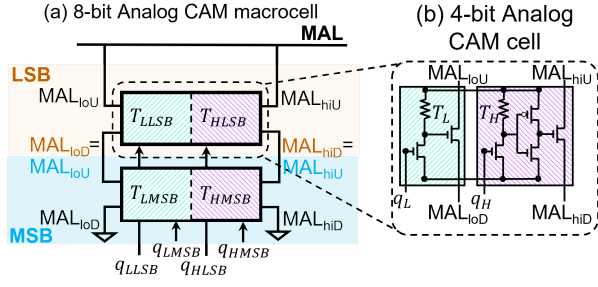


Fig. 5. (a) analog CAM 8-bit macro-cell and (b) analog CAM 4-bit sub-cell circuit.

used for directly accessing the SRAM WLs. The SRAM stores the corresponding leaf value of each branch, which is retrieved sequentially and accumulated by the ACC block, which performs a *local* reduction operation. After $N_{trees,core}$ accumulations are performed, the resulting leaf value is sent as output to the router. Leaf values coming from multiple cores can be summed at the router level as section III-D discusses, performing a *shared* reduction operation. Finally, the resulting leaf value is propagated to the CP which performs a *global* reduction and computes the model prediction. The latter is usually a simple operation, such as a majority voting or a threshold comparison.

B. Analog CAM with improved precision

ML algorithms usually do not require high-precision floating point operations for achieving good results [29]. As will be detailed in section IV we found out that typically 8 bits precision, corresponding to 256 bins for each feature, is required for matching floating point (FP) accuracy inference of tree-based ML models.

While analog CAM circuits offer the possibility of mapping arbitrary ranges, memristor device reliability poses a challenge in supporting more than 16 levels or 4 bits [15]. In the case of crossbar arrays of memristors mapping algebraic matrices, such as a neural network layer, multiple techniques have been proposed for overcoming limited device precision. For example, with bit slicing [11] by using M levels memristor, $N = 2^{2M}$ bits can be represented by connecting two devices on the same row. In crossbar arrays, it is also straightforward to arbitrarily adjust the input precision by applying binary pulses and performing SHIFT and ADD operations at the output [11].

Unfortunately, such techniques do not apply to analog CAM arrays. The analog CAM encodes a *unary* representation and by connecting two analog CAM cells on the same MAL to represent one macro-cell, it is only possible to double the number of levels (i.e. $2^{N_{bits}}$) rather than the number of bits. Thus given memristors with $M = 4$ bits, **16** analog CAM cells are needed for representing $N = 8$ bits, leading to an exponential overhead. Here, we propose a novel solution to increase the precision with the same base analog CAM cell circuit, which requires 2 analog CAM cells and 2 clock cycles for performing 8-bit search operation with $M = 4$ bits memristors.

To demonstrate, let us first take the case where the lower bound threshold T_L is needed to be mapped and operated with $N = 8$ bit of precision but we only have $M = 4$ bits of precision in our analog CAM and memristor devices. The lower bound threshold can be sub-divided into its most significant bit representation T_{LMSB} and least significant bit representation T_{LLSB} , each one made of M bits and written as $T_L = 2^M T_{LMSB} + T_{LLSB} = 16T_{LMSB} + T_{LLSB}$. Each analog CAM cell computes the conditional operation $MAL = q \geq T_L$, where q is the input query applied to the DL. We similarly divide the input q into most and least significant representations q_{MSB} and q_{LSB} , such that $q = 2^M q_{MSB} + q_{LSB} = 16q_{MSB} + q_{LSB}$ and we can obtain the result of MAL by computing

$$[(q_{MSB} \geq T_{LMSB}) \wedge (q_{LSB} \geq T_{LLSB})] \vee (q_{MSB} \geq T_{LMSB} + 1) \quad (2)$$

or alternatively, rearranging the terms:

$$[(q_{MSB} \geq T_{LMSB} + 1) \vee (q_{LSB} \geq T_{LLSB})] \wedge (q_{MSB} \geq T_{LMSB}). \quad (3)$$

Note that Eq. 3 is more CAM-friendly since it is a conjunction of two terms that can be appended to the same MAL. The same calculation derives the upper bound T_H conditions and with an AND operation between this and equation (3), the full computation $MAL = T_L \leq q < T_H$ results in:

$$[(q_{MSB} \geq T_{LMSB} + 1) \vee (q_{LSB} \geq T_{LLSB})] \wedge (q_{MSB} \geq T_{LMSB}) \wedge [(q_{MSB} < T_{HMSB}) \vee (q_{LSB} < T_{HLSB})] \wedge (q_{MSB} < T_{HMSB} + 1). \quad (4)$$

Analog CAMs cells arranged on the same MAL perform a bit-wise AND (\wedge) operation between them, thus a circuit addition is needed for performing the OR (\vee) operation. To do that we realized analog CAM macro-cells as shown in Fig. 5(a). Each analog CAM macro-cell is made of two sub-cells (Fig. 5(b)), which are equivalent to the circuit design previously presented [14], [15]. These sub-cells are connected such that the LSB cell has upper MALs (MAL_{loU} and MAL_{hiU}) connected to the principal MAL of the row (which is shared among multiple columns), bottom MALs connected to the upper MALs of the MSB cell, while the MSB cell has its bottom MALs connected to ground, as shown in Fig. 5. In this configuration, the macro-cell implements an OR operation with analog CAM sub-cells. Effectively, the MAL stays charged high for a match if either the MSB sub-cell or the LSB sub-cell is matched. However, to perform the operation of equation (4), inputs on the lower and upper thresholds must be separated, thus each DL is an analog bus of 4 wires. While this could signal a large overhead, in practice these two lines are already independent and separated in the original analog CAM circuit to enable programming of the memristor devices [14].

Table I shows the required inputs for each DL analog bus wire to compute equation (4) in a 2-step search operation. With MAL pre-charged high, the first cycle evaluates the first bracket of equation (4) for the lower and upper bound (the OR operation). Without pre-charging MAL again, the second

TABLE I
INPUT TO APPLY FOR DOUBLING PRECISION WITH TIME SHIFTING

Input	Cycle 1	Cycle 2
q_{HLSB}	q_{LSB}	GND
q_{LLSB}	q_{LSB}	VDD
q_{HMSB}	q_{MSB}	$q_{MSB} - 1$
q_{LMSB}	$q_{MSB} - 1$	q_{MSB}

cycle evaluates the second term of each bound by inputting *always care* (i.e. always mismatch) values to the LSB sub-cell. Therefore, an AND operation between the outputs of cycle 1 and cycle 2 is computed on MAL following cycle 2, similar to a 2-step search approach previously demonstrated for increasing bit density in TCAMs [30].

To the best of our knowledge, this is an entirely new approach and the proposed circuit operation is the most compact way of computing equation (4) with an analog CAM, and thus for doubling the bit precision. While other circuit designs may implement the same function in one clock cycle, these would have a significantly larger area. For example, one could separate cells performing the OR operation by connecting the discharge transistors in series rather than in parallel. This approach would also allow for selecting the precision of each feature to be either 4 or 8-bit, depending on the required precision. However, to perform such an operation in one cycle, three analog CAM cells with complex routing are needed. Given that analog CAM search latency is forecast to 100 ps [14], we found that performing two searches rather than one would not unduly increase the overall latency. Thus, we adopt this circuit formulation and operation which doubles the bit precision while doubling the area and analog CAM search latency.

C. Core pipeline

In our ML experiments and hyperparameters search (see IV-A for details) we found out that $N_{leaves} = 256$ per tree is typically sufficient to achieve high accuracy. Given that previous results have shown that analog CAM arrays with up to 128 rows do not encounter significant technology issues at 16 nm [14], each X-TIME core contains 2 stacked arrays, resulting in $2 \times 128 = 256$ addressable words (N_{leaves}). We perform a survey on the size of typical tabular datasets [1], finding that usually $N_{feat} < 100$ and often feature pre-processing reduces the number of N_{feat} significantly before applying inputs to the decision tree ensemble. Previous results have shown that arrays with up to 100 columns have a very small access latency (< 1 ns) [14]. Nevertheless, we include an outlier dataset with $N_{feat} = 130$ [31] to show how to handle larger input vector sizes with input vector segmentation, as will be described below. Each core contains 2 arrays of 65 columns, resulting in a width of $2 \times 65 = 130$. Overall, each core has a total addressable analog CAM of macro array size $2 \times 128 \times 2 \times 65 = 256 \times 65$.

The search operation is performed in series by groups of 65 features, while all the branches mapped to each queued array are computed in parallel. Multiple trees can be mapped

to a single core, by arranging them in different portions of the analog CAM macro on the vertical axis. To avoid structural hazards, different considerations are made before applying new inputs to the core, as will be discussed below. When a feature vector is searched, a set of components with indices ranging from 0 to 64 is sent to the first analog CAM logical array (aCAM1) while a second set of components with indices from 65 to 129 is sent to the second array (aCAM2). Comparison sequences on each tree branch are reconstructed by the AND operations made by aCAM1 and aCAM2 by selectively pre-charging only aCAM2 rows matched in aCAM1. Each analog CAM array has a latency of $\lambda_{CAM} = 4$ cycles for performing the search operation. One cycle is used for pre-charging the MAL, two cycles for the search operation (MSB and LSB), and one cycle for latching the MAL sense amp, which leads to a total core latency of $\lambda_C = 12$ cycles, with all other components (Buffer, MMR, SRAM, ACC) having a single cycle latency.

In the case of up to four trees mapped to the core when an array finishes the search operation, it starts processing a new sample and no additional bubbles are required. The maximum ideal core throughput τ_C , considering a clock frequency of 1GHz [14] and a relatively large number of samples N_s , can thus be computed by

$$\tau_C = \frac{N_s}{\lambda_C + \lambda_{CAM}(N_s - 1)} \sim 250M\text{Samples/s}. \quad (5)$$

If more than 4 trees are mapped in the core, extra pipeline bubbles $N_B = N_{trees,core}$ should be inserted. In fact, the MMR needs to perform more than 4 iterations in order to generate the one-hot vector for accessing the leaves, stored in the SRAM. The core pipeline in this case reaches an ideal throughput of

$$\tau_C = \frac{N_s}{\lambda_C + N_B(N_s - 1)} \sim 200M\text{Samples/s} \quad (6)$$

To maintain such a high throughput, cores need to be fed with input data fast enough. On the other hand, the architecture should be able to adapt to multiple models (such as RF, XGBoost, and others, either classification or regression problems) and exploit the vast amount of cores for parallel computations. Thus we designed a programmable NoC able to handle multiple workloads.

D. Flexible connectivity

We identified four possible examples of inference operation that cover all ensemble models and tasks previously described, and exploit all the possibilities of our architecture: (1) regression and binary classification, (2) multi-class classification, (3) regression and binary classification with input batching and (4) multi-class classification with input batching.

In the case of regression and binary classification, leaves contain normalized partial predictions of each tree branch called *logits*, that are summed over the ensemble. In each core, the SRAM is programmed with logits that are summed locally in the core and in each network node inside the router. The final prediction is then sent to the CP which compares it with a threshold, typically 0 or 0.5, and sends the final result to the

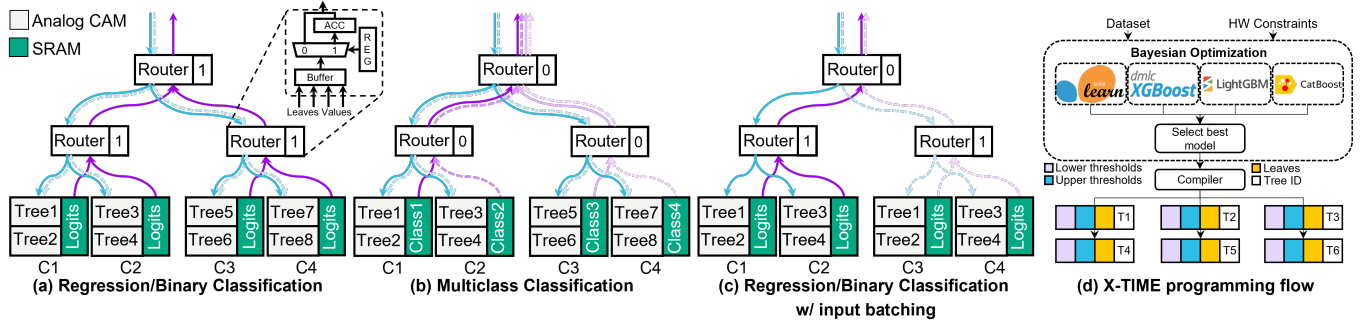


Fig. 6. Example of network configurations for regression/binary classification (a), multiclass classification (b) and regression/binary classification with input batching (c). (d) Schematic representation of X-TIME programming flow

output. In the case of multiclass classification, logits should be summed class-wise and N_{class} logits should be sent to the CP which performs an *argmax* computation to select the predicted class.

We propose a flexible/re-configurable NoC design (Fig. 6(a-c)) to aggregate results based on model type. The inset of Fig. 6(a) shows the downstream circuit schematic for the custom router. A buffer stores incoming leaves and has the output connected to a de-multiplexer (DEMUX) controlled by a configuration register. The DEMUX sends each leaf either to the accumulator circuit or directly to the output, with only logits belonging to the same class accumulated. Three examples of network configuration are shown in Fig. 6 for supporting (a) regression or binary classification, (b) multiclass classification, and (c) regression or binary classification with input batching. In the first case, the X-TIME compiler maps $N_{trees} = 8$ trees with a depth $D = 7$ each, with $N_{trees,core} = 2$ each core. The same inputs (blue solid and light blue dashed lines) are applied to all the cores in parallel and all the logits (solid purple lines) are summed together, being a regression/binary classification problem. The X-TIME compiler sets the configuration bit of all routers to '1' such that logits are always accumulated in the router before propagating.

For multi-class classification (Fig. 6(b)), the X-TIME compiler maps $N_{estimators} = 2$ estimators each made of $N_{trees} = 4$ (one for each class) with a depth $D = 7$. Each core holds two trees belonging to the same class and the same inputs (blue solid and light blue dashed lines) are applied to all cores in parallel. The X-TIME compiler sets router configuration bits to 0, as it is not possible to perform an accumulation/reduction at the router level and the reduction must be done globally by the CP. Thus, logits for each class are transmitted independently (solid purple lines, dashed purple lines, solid pink lines, and dashed pink lines).

Finally, for regression/binary classification with input batching (Fig. 6(c)), the X-TIME compiler maps an ensemble of $N_{trees} = 4$ with depth $d = 7$ and to increase the throughput, replicates trees in multiple cores, such that cores C1 and C2 map the same trees of cores C3 and C4. Different inputs are applied to different cores, or groups of cores by appropriately addressing each feature vector. Core C1 and C2 receive a first input (solid blue line) while cores C3 and C4 receive a second input (dashed light blue). Logits can be accumulated at the

router level only between trees belonging to the same input batch, as in the lower level of the architecture in Fig. 6(c). The X-TIME compiler programs the lower level router configuration bits to '1' to enable local accumulation, and the higher level configuration bits to '0' to enable logits direct propagation. Input batching addresses one of the main issues of specialized accelerators in keeping resource utilization high [32]. With a similar procedure, multiple unique models can be mapped to the accelerator, by assigning a different batch to each model.

IV. EVALUATION METHODOLOGY

A. Datasets and model training

For our experiments, we trained state-of-the-art models with three ML algorithms on a set of benchmark datasets (details in Table II). The algorithms included random forests (RF) from scikit-learn [28], and gradient boosted trees from XGBoost [17], and CatBoost [18]. Fig. 6(d) shows a conceptual schematic of the workflow, whose output is a series of threshold maps (one for each tree) with the lower/upper bound to program in analog CAMs, the corresponding core/class address and leaf value for each node.

B. Cycle-detailed simulator

We developed a functional and cycle-detailed simulator¹ to evaluate latency, throughput, energy efficiency, area, and accuracy of the in-memory engine for tree-based model inference. The architecture simulator was developed using the Structural Simulation Toolkit (SST) [39] and estimates the performance on the benchmark datasets detailed above. SST, which is a parallel discrete-event simulator framework, can integrate modular components in a unified interface and simulate large-scale systems with MPI. It also provides interfaces for simulation components and components that perform actual functions such as processors, memory, and networks. For our system, the user-defined components emulate the cycle-level function of each block described in Fig. 4, and data flow through the links connecting the components with specified delay. The cycle-level architecture simulation consisting of an H-tree NoC with 4096 cores and 1365 routers verified the error-free functional

¹<https://github.com/HewlettPackard/X-TIME>

TABLE II
DATASETS AND MODELS CHARACTERIZATION

Dataset	ID	Task	Samples	N_{feat}	$N_{classes}$	Model	N_{trees}	$N_{leaves,max}$
Churn modelling [33]	1	Binary Classification	10000	10	2	CatBoost	404	256
Eye movements [34]	2	Multiclass Classification	10936	26	3	XGBoost	2352	256
Forest cover type [35]	3	Multiclass Classification	581012	54	7	XGBoost	1351	231
Gas concentration [31]	4	Multiclass Classification	13910	129	6	Random Forest	1356	217
Gesture phase segmentation [36]	5	Multiclass Classification	9873	32	5	XGBoost	1895	256
Telco customer churn [37]	6	Binary Classification	7032	19	2	XGBoost	159	4
Rossmann stores sales [38]	7	Regression	610253	29	N/A	XGBoost	2017	256

operation and the pipelined architecture without hazards, while also yielding system performance estimates. Fig. 7 summarizes

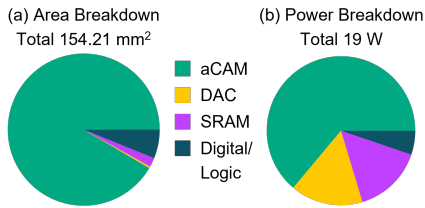


Fig. 7. Area (a) and peak power (b) breakdown

the power and area for the proposed architecture. Previous work generated layouts for the analog CAM at 16 nm [14], [15], which included the analog CAM array, DAC, SA, and P-Ch area, and extracted power consumption using single cell parameters [15]. The analog CAM model was previously validated by experimental measurements [14]. Here, we simulate model mapping using memristor conductances from $1\mu S$ to $100\mu S$. The analog CAM model also includes parasitics that limit the CAM pre-charge and discharge time and the DAC operational frequency [14]. Power and area values for register and logic are based on TSMC 16nm PDK. The MMR design is based on the matching token MMR topology [40] whose output is fed back to MAL registers enabling multiple iterations when multiple trees are mapped to the same core. Notably, the analog CAM arrays dominate area and power consumption, with peripheral components contributing negligibly. Also, the overall peak power consumption of 19 W is comparable to GPU idle power (~ 25 W).

C. Profiling Tree Model Inference on NVIDIA GPUs, FPGA and SRAM based accelerators

To demonstrate the analog CAM performance capabilities, we compare our results to three alternative accelerator approaches: GPU, FPGA, and digital SRAM. As our first performance baseline, we profiled the inference step of the tree models and corresponding datasets shown in Table II on an NVIDIA V100 GPU. We measured each GPU kernel execution time with 5 repetitions to process data batches of increasing size, up to a saturation point, where throughput improvements were no longer observed. To estimate GPU upper bound performance, we isolated the kernel execution time of each model using NVIDIA’s *nvprof* tool, and did not include the memory transfer times between host (CPU) to device (GPU) or internal GPU transfers in our measured times.

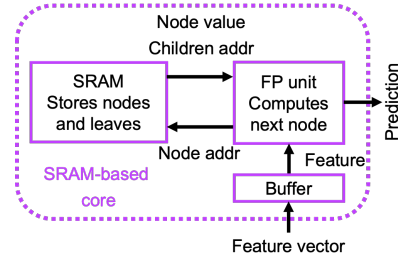


Fig. 8. Schematic of the SRAM-based accelerator core used as digital baseline.

When possible, we profiled models using CUDA kernels from the NVIDIA RAPIDS Forest Inference Library (FIL).

Moreover, we compared X-TIME with an FPGA baseline FAXID [8]. FAXID is a custom hardware accelerator for low-latency ransomware detection using high-level synthesis (HLS) using binary classification models. As FAXID only supports binary classification, for our comparison we used a 1-vs-all approach to benchmark latency and throughput where we select one of the classes as class 0 and set the remaining classes to class 1. In FAXID the maximum depth was restricted to 6, as their ransomware detection accuracy did not increase with deeper trees. To keep the baseline results faithful to the FAXID HLS design, we optimized the hyperparameters of Table II for smaller depth and larger number of trees on FAXID to match accuracy with the other approaches.

Finally, we compare X-TIME to a custom digital accelerator baseline using SRAM to isolate the performance benefits from the analog CAM specifically. This SRAM baseline uses a distributed architecture with each tree mapped to a small SRAM accessed serially by a floating point unit [5], as shown in Fig. 8. Each SRAM word stores the node value and feature, the left and right children addresses, or the corresponding logic or class in the case of a leaf node. We considered the X-TIME network architecture and changed just the core operation (analog CAM or digital SRAM) to simulate the effect on throughput, of multiple accesses required for each tree.

One might consider a digital TCAM to be another meaningful comparison. However, as previously demonstrated [41], using a traditional digital TCAM for performing on-access comparison would result in large overheads. In detail, 2^8 TCAM columns would be needed to represent each feature with 8-bit precision, and thus tree inference of 129 features requires 33024 TCAM columns. Considering an 80-column

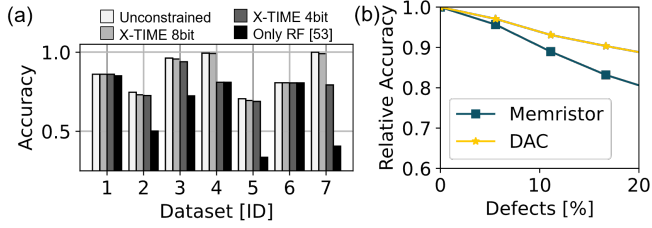


Fig. 9. (a) Accuracy for different training constraints and (b) relative accuracy as a function of memristor and DAC defects.

TCAM macro has an access time of $\sim 500ps$ [42], inference with a TCAM would take $500 \cdot 33024/80ps \approx 20us$ per tree, significantly larger than the few cycles analog CAM latency.

V. RESULTS

A. Model inference performance

In designing our HW architecture, we investigated the required bit accuracy and model types that the architecture should support to maintain state-of-the-art model accuracy. To assess these parameters, we compared model accuracy for different training parameters and model types to guide the X-TIME requirements (Fig. 9(a)). First, we set our baseline, achieving state-of-the-art accuracy [43] by training all the models without constraints in the hyperparameters search ('Unconstrained' in Fig. 9(a)). We then optimized models to fit the hardware using the proposed 8-bit precision ACAM ('X-TIME 8bit': maximum $N_{trees} = 4096$, $N_{leaves,max} = 256$, $N_{bit} = 8$), which resulted in limited accuracy loss compared to the unconstrained baseline case. To assess the need for 8-bit vs. 4-bit analog CAMs, we optimized the model to fit hardware using a 4-bit ACAM [15], allowing the number of leaves to double, such that the area would be equivalent to 'X-time 8bit' ('X-TIME 4bit': maximum $N_{trees} = 4096$, $N_{leaves,max} = 512$, $N_{bit} = 4$). Another option would double the maximum number of allowed trees, but we generally found that 4096 trees are high enough for matching unconstrained baseline accuracy. Our results showed a reduction in performance of 20% in the case of regression on Rossmann store sales dataset [38] and 18% in the case of multi-class classification on gas concentration dataset [31]. Finally, we limited the optimizer to RF models only, which resulted in significant accuracy degradation for several datasets (label = 'Only RF'). Given that it is not possible to train directly with 4-bit precision, the after-training quantization significantly decreased accuracy, demonstrating the need for supporting a broader range of model types beyond those demonstrated in previous works [15], [44].

To assess the promise of this analog hardware approach in practical use, we also studied the impact of variations and defects of the analog hardware on model inference accuracy. The two most impactful sources of error to classification/regression results in this analog hardware are the known memristor conductance variations and DAC input variations to the aCAM. We considered experimental data from TaOx memristor and 16 nm analog circuits [15]. Fig. 9(b) shows the mean relative

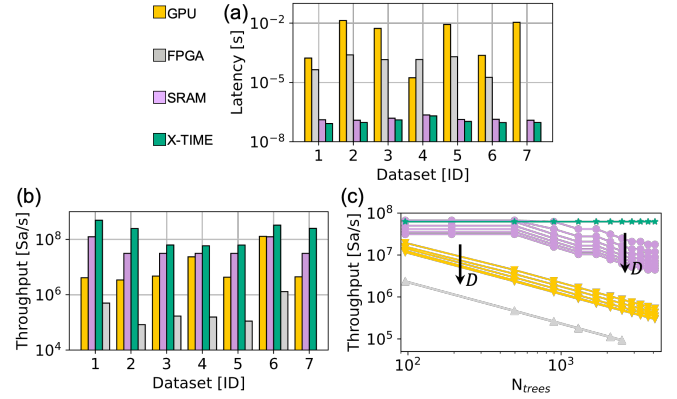


Fig. 10. Comparison of (a) latency and (b) throughput of this work, GPU, FPGA, and SRAM based accelerator from Fig. 8 (a) Throughput as a function of N_{trees} and D .

accuracy, defined as the ideal accuracy of Fig. 9(a) over the defect-compromised accuracy as a function of the percentage of defects. We defined a defect as a 1-level random flip in the memristor conductance or DAC output voltage.

The plot shows the average results across all classification datasets. We observe that these models and our architecture are fairly resilient to memristor variations, as individual errors do not have a large impact due to the ensemble nature of the model itself. With the aforementioned conductance window and a conservative standard deviation of $1\mu S$ it is expected to have a flip probability of $\sim 0.2\%$, corresponding to accuracy drop $< 0.5\%$. On the other hand, while DAC variations also impact the accuracy, DACs are usually designed for operating up to 16 bits [45], thus realizing a stable/error-free 4-bit design is not particularly challenging.

B. Comparison with state-of-the-art

We benchmarked our proposed architecture on a wide range of models (corresponding to X-TIME 8bit of Fig. 9) and dataset types (Table II), and compared latency and throughput (see Fig. 10(a,b)) to GPU, FPGA and a digital accelerator based on small SRAMs and similar to Booster [5]. When possible, we applied input batching and replicated trees to increase throughput. As shown, our architecture produces drastically reduced latency, frequently to $\sim 100ns$ compared to GPU at $10\mu s$ to ms, while also demonstrating significantly improved throughput by 10-120 \times across most datasets. Our architecture shines for large binary classification or regression models with a peak improvement in latency by 9740 \times at 119 \times higher throughput for the Churn modeling dataset inference [33] compared to GPU. As tree search is parallel in each analog CAM array of each core, as well as the in-network reduction, latency, and throughput are constant with N_{trees} and N_{leaves} with a delay solely dependant on N_{feat} and $N_{classes}$. In contrast, on GPU there is a linear dependence on N_{trees} and D , which limits the performance for large models. In the FPGA implementation, namely FAXID, there is a linear dependence on N_{trees} . The SRAM-based accelerator has a linear dependence on D (since multiple memory accesses

are required) and N_{trees} when more than a tree needs to be mapped in a core. As an example, we studied the throughput as a function of N_{trees} and D for GPU, FPGA, SRAM-based accelerator, and X-TIME as shown in Fig. 10(c), for a multiclass classification dataset [35], demonstrating the predicted trend. We note that the SRAM-based accelerator still suffers from load imbalance between trees, similar to GPU, in which trees with different depths have different inference times, which results in the need for synchronization before the reduction operation. The high throughput of X-TIME can produce an extremely low energy per decision, down to 0.3 nJ/Dec, highlighting the potential for energy-efficient applications.

VI. CONCLUSIONS

In this work, we presented a novel architecture for accelerated tree-based ML inference with in-memory computing based on a novel increased precision analog non-volatile CAMs. Our approach maps decision trees to analog CAM ranges, which compute directly the matched results in parallel given an input feature vector. Leaf values are stored in a local SRAM and accumulated at the core level when multiple trees are mapped in the same core. Outside the core, an H-tree NoC connects 4096 cores and a co-processor in a single chip. An in-network computing structure accumulates leaf values as data flows to limit data movement. The on-chip network is re-configurable to map different models (regression, multiclass classification, etc) and inference techniques, such as input batching. Our results show significant improvement in latency – by almost four orders of magnitude, compared with an NVIDIA V100 GPU, at a throughput up to $\sim 120\times$ higher across a wide range of dataset types and model topologies.

VII. REFERENCES

REFERENCES

- [1] L. Grinsztajn, E. Oyallon, and G. Varoquaux, “Why do tree-based models still outperform deep learning on typical tabular data?” in *Advances in Neural Information Processing Systems, Datasets and Benchmarks Track*. Curran Associates, Inc., 2022.
- [2] S. M. Lundberg, G. Erion, H. Chen, A. DeGrave, J. M. Prutkin, B. Nair, R. Katz, J. Himmelfarb, N. Bansal, and S.-I. Lee, “From local explanations to global understanding with explainable AI for trees,” *Nature Machine Intelligence*, vol. 2, no. 1, pp. 56–67, Jan. 2020.
- [3] “State of data science and machine learning 2021,” <https://www.kaggle.com/kaggle-survey-2021>, accessed: 2022-07-25.
- [4] Z. Xie, W. Dong, J. Liu, H. Liu, and D. Li, “Tahoe: tree structure-aware high performance inference engine for decision tree ensemble on GPU,” in *Proceedings of the Sixteenth European Conference on Computer Systems*. ACM, Apr. 2021, pp. 426–440.
- [5] M. He, M. Thottethodi, and T. N. Vijaykumar, “Booster: An accelerator for gradient boosting decision trees training and inference,” in *2022 IEEE International Parallel and Distributed Processing Symposium (IPDPS)*, 2022, pp. 1051–1062.
- [6] “Ieee-cis fraud detection competition,” <https://www.kaggle.com/code/cdeotte/xgb-fraud-with-magic-0-9600/notebook>, accessed: 2022-10-10.
- [7] S. Summers, G. D. Guglielmo, J. Duarte, P. Harris, D. Hoang, S. Jindariani, E. Kreinar, V. Loncar, J. Ngadiuba, M. Pierini, D. Rankin, N. Tran, and Z. Wu, “Fast inference of Boosted Decision Trees in FPGAs for particle physics,” *Journal of Instrumentation*, vol. 15, no. 05, pp. P05 026–P05 026, May 2020, publisher: IOP Publishing.
- [8] A. Gajjar, P. Kashyap, A. Aysu, P. Franzon, S. Dey, and C. Cheng, “Faxid: Fpga-accelerated xgboost inference for data centers using hls,” in *2022 IEEE 30th Annual International Symposium on Field-Programmable Custom Computing Machines (FCCM)*, 2022, pp. 1–9.
- [9] G. Tzimpragos, A. Madhavan, D. Vasudevan, D. Strukov, and T. Sherwood, “Boosted race trees for low energy classification,” in *Proceedings of the Twenty-Fourth International Conference on Architectural Support for Programming Languages and Operating Systems*, ser. ASPLOS ’19. New York, NY, USA: Association for Computing Machinery, 2019, p. 215–228.
- [10] M. A. Zidan, J. P. Strachan, and W. D. Lu, “The future of electronics based on memristive systems,” *Nature Electronics*, vol. 1, no. 1, pp. 22–29, Jan. 2018.
- [11] A. Shafiee, A. Nag, N. Muralimanohar, R. Balasubramonian, J. P. Strachan, M. Hu, R. S. Williams, and V. Srikumar, “ISAAC: A Convolutional Neural Network Accelerator with In-Situ Analog Arithmetic in Crossbars,” in *2016 ACM/IEEE 43rd Annual International Symposium on Computer Architecture (ISCA)*. Seoul, South Korea: IEEE, Jun. 2016, pp. 14–26. [Online]. Available: <http://ieeexplore.ieee.org/document/7551379/>
- [12] K. Pagiamtzis and A. Sheikholeslami, “Content-Addressable Memory (CAM) Circuits and Architectures: A Tutorial and Survey,” *IEEE Journal of Solid-State Circuits*, vol. 41, no. 3, pp. 712–727, Mar. 2006.
- [13] C. E. Graves, C. Li, G. Pedretti, and J. P. Strachan, “In-Memory Computing with Non-volatile Memristor CAM Circuits,” in *Memristor Computing Systems*, L. O. Chua, R. Tetzlaff, and A. Slavova, Eds. Cham: Springer International Publishing, 2022, pp. 105–139.
- [14] C. Li, C. E. Graves, X. Sheng, D. Miller, M. Foltin, G. Pedretti, and J. P. Strachan, “Analog content-addressable memories with memristors,” *Nature Communications*, vol. 11, no. 1, p. 1638, Dec. 2020.
- [15] G. Pedretti, C. E. Graves, S. Serebryakov, R. Mao, X. Sheng, M. Foltin, C. Li, and J. P. Strachan, “Tree-based machine learning performed in-memory with memristive analog CAM,” *Nature Communications*, vol. 12, no. 1, p. 5806, Oct. 2021.
- [16] G. Biau and E. Scornet, “A random forest guided tour,” *TEST*, vol. 25, no. 2, pp. 197–227, Jun. 2016.
- [17] T. Chen and C. Guestrin, “XGBoost: A Scalable Tree Boosting System,” in *Proceedings of the 22nd ACM SIGKDD International Conference on Knowledge Discovery and Data Mining*. San Francisco California USA: ACM, Aug. 2016, pp. 785–794.
- [18] L. Prokhorenkova, G. Gusev, A. Vorobev, A. V. Dorogush, and A. Gulin, “CatBoost: unbiased boosting with categorical features,” in *Advances in Neural Information Processing Systems*, S. Bengio, H. Wallach, H. Larochelle, K. Grauman, N. Cesa-Bianchi, and R. Garnett, Eds., vol. 31, 2018.
- [19] S. Raschka, J. Patterson, and C. Nolet, “Machine learning in python: Main developments and technology trends in data science, machine learning, and artificial intelligence,” *arXiv preprint arXiv:2002.04803*, 2020.
- [20] Q. Guo, X. Guo, Y. Bai, and E. İpek, “A resistive TCAM accelerator for data-intensive computing,” in *Proceedings of the 44th Annual IEEE/ACM International Symposium on Microarchitecture - MICRO-44 ’11*. Porto Alegre, Brazil: ACM Press, 2011, p. 339.
- [21] C. E. Graves, C. Li, X. Sheng, D. Miller, J. Ignowski, L. Kiyama, and J. P. Strachan, “In-Memory Computing with Memristor Content Addressable Memories for Pattern Matching,” *Advanced Materials*, vol. 32, no. 37, p. 2003437, Sep. 2020.
- [22] H. Li, W.-C. Chen, A. Levy, C.-H. Wang, H. Wang, P.-H. Chen, W. Wan, W.-S. Khwa, H. Chuang, Y.-D. Chih, M.-F. Chang, H.-S. P. Wong, and P. Raina, “SAPIENS: A 64-kb RRAM-Based Non-Volatile Associative Memory for One-Shot Learning and Inference at the Edge,” *IEEE Transactions on Electron Devices*, vol. 68, no. 12, pp. 6637–6643, 2021.
- [23] D. Ielmini and H.-S. P. Wong, “In-memory computing with resistive switching devices,” *Nature Electronics*, vol. 1, no. 6, pp. 333–343, Jun. 2018.
- [24] A. S. Rekhi, B. Zimmer, N. Nedovic, N. Liu, R. Venkatesan, M. Wang, B. Khailany, W. J. Dally, and C. T. Gray, “Analog/Mixed-Signal Hardware Error Modeling for Deep Learning Inference,” in *Proceedings of the 56th Annual Design Automation Conference 2019*, ser. DAC ’19. New York, NY, USA: Association for Computing Machinery, 2019, event-place: Las Vegas, NV, USA.
- [25] K. Ni, X. Yin, A. F. Laguna, S. Joshi, S. Dünkel, M. Trentzsch, J. Müller, S. Beyer, M. Niemier, X. S. Hu, and S. Datta, “Ferroelectric ternary content-addressable memory for one-shot learning,” *Nature Electronics*, vol. 2, no. 11, pp. 521–529, Nov. 2019.
- [26] G. Pedretti, C. E. Graves, T. Van Vaerenbergh, S. Serebryakov, M. Foltin, X. Sheng, R. Mao, C. Li, and J. P. Strachan, “Differentiable Content Addressable Memory with Memristors,” *Advanced Electronic Materials*, p. 2101198, 2022.
- [27] M. Kang, S. K. Gonugondla, S. Lim, and N. R. Shanbhag, “A 19.4-nJ/Decision, 364-K Decisions/s, In-Memory Random Forest Multi-Class

- Inference Accelerator,” *IEEE Journal of Solid-State Circuits*, vol. 53, no. 7, pp. 2126–2135, Jul. 2018.
- [28] F. Pedregosa, G. Varoquaux, A. Gramfort, V. Michel, B. Thirion, O. Grisel, M. Blondel, P. Prettenhofer, R. Weiss, V. Dubourg, J. Vanderplas, A. Passos, D. Cournapeau, M. Brucher, M. Perrot, and E. Duchesnay, “Scikit-learn: Machine learning in Python,” *Journal of Machine Learning Research*, vol. 12, pp. 2825–2830, 2011.
- [29] S. Gupta, A. Agrawal, K. Gopalakrishnan, and P. Narayanan, “Deep Learning with Limited Numerical Precision,” in *Proceedings of the 32nd International Conference on Machine Learning*, ser. Proceedings of Machine Learning Research, F. Bach and D. Blei, Eds., vol. 37. Lille, France: PMLR, Jul. 2015, pp. 1737–1746.
- [30] C.-C. Lin, J.-Y. Hung, W.-Z. Lin, C.-P. Lo, Y.-N. Chiang, H.-J. Tsai, G.-H. Yang, Y.-C. King, C. J. Lin, T.-F. Chen, and M.-F. Chang, “7.4 A 256b-wordlength ReRAM-based TCAM with 1ns search-time and 14× improvement in wordlength-energyefficiency-density product using 2.5T1R cell,” in *2016 IEEE International Solid-State Circuits Conference (ISSCC)*, 2016, pp. 136–137.
- [31] A. Vergara, S. Vembu, T. Ayhan, M. A. Ryan, M. L. Homer, and R. Huerta, “Chemical gas sensor drift compensation using classifier ensembles,” *Sensors and Actuators B: Chemical*, vol. 166–167, pp. 320–329, 2012.
- [32] C. Xu, A. Lain, P. Faraboschi, N. Dube, and D. Milojicic, “Feeding the beast: High performance data pipeline for large-scale deep learning,” in *A Collection of White Papers from the BDEC2 Workshop in San Diego, California*, vol. 1, 2019, p. 14.
- [33] S. Iyer, “Churn modelling,” accessed: 2022-07-26. [Online]. Available: <https://www.kaggle.com/datasets/shrutimechlearn/churn-modelling>
- [34] J. Salojärvi, K. Puolamäki, J. Simola, L. Kovanen, I. Kojo, and S. Kaski, “Inferring relevance from eye movements: Feature extraction,” in *Workshop at NIPS 2005, in Whistler, BC, Canada, on December 10, 2005.*, 2005, p. 45.
- [35] J. A. Blackard and D. J. Dean, “Comparative accuracies of artificial neural networks and discriminant analysis in predicting forest cover types from cartographic variables,” *Computers and electronics in agriculture*, vol. 24, no. 3, pp. 131–151, 1999.
- [36] P. K. Wagner, S. M. Peres, R. C. B. Madeo, C. A. de Moraes Lima, and F. de Almeida Freitas, “Gesture unit segmentation using spatial-temporal information and machine learning,” in *The Twenty-Seventh International Flairs Conference*, 2014.
- [37] BlastChar, “Telco customer churn,” accessed: 2022-07-26. [Online]. Available: <https://www.kaggle.com/datasets/blastchar/telco-customer-churn>
- [38] “Rossmann store sales kaggle competition: forecast sales using store, promotion, and competitor data,” accessed: 2022-07-26. [Online]. Available: <https://www.kaggle.com/competitions/rossmann-store-sales/overview>
- [39] A. F. Rodrigues, K. S. Hemmert, B. W. Barrett, C. Kersey, R. Oldfield, M. Weston, R. Risen, J. Cook, P. Rosenfeld, E. Cooper-Balis, and B. Jacob, “The Structural Simulation Toolkit,” *SIGMETRICS Perform. Eval. Rev.*, vol. 38, no. 4, pp. 37–42, Mar. 2011, place: New York, NY, USA Publisher: Association for Computing Machinery.
- [40] N. Mohan, W. Fung, D. Wright, and M. Sachdev, “Design techniques and test methodology for low-power tcams,” *IEEE Transactions on Very Large Scale Integration (VLSI) Systems*, vol. 14, no. 6, pp. 573–586, 2006.
- [41] R. M. Roth, “On the implementation of boolean functions on content-addressable memories,” in *2023 IEEE International Symposium on Information Theory (ISIT)*, 2023, pp. 1408–1413.
- [42] Y. Tsukamoto, M. Morimoto, M. Yabuuchi, M. Tanaka, and K. Nii, “1.8 mbit/mm² ternary-cam macro with 484 ps search access time in 16 nm fin-fet bulk cmos technology,” in *2015 Symposium on VLSI Circuits (VLSI Circuits)*, 2015, pp. C274–C275.
- [43] R. Shwartz-Ziv and A. Armon, “Tabular data: Deep learning is not all you need,” *Information Fusion*, vol. 81, pp. 84–90, 2022.
- [44] L. Zhao, Q. Deng, Y. Zhang, and J. Yang, “Rfacc: A 3d reram associative array based random forest accelerator,” in *Proceedings of the ACM International Conference on Supercomputing*, ser. ICS ’19. New York, NY, USA: Association for Computing Machinery, 2019, p. 473–483.
- [45] C.-H. Lin, K. L. J. Wong, T.-Y. Kim, G. R. Xie, D. Major, G. Unruh, S. R. Dommaraju, H. Eberhart, and A. Venes, “A 16b 6gs/s nyquist dac with imd \leq -90dbc up to 1.9ghz in 16nm cmos,” in *2018 IEEE International Solid - State Circuits Conference - (ISSCC)*, 2018, pp. 360–362.

VIII. BIOGRAPHY SECTION

Giacomo Pedretti (Member, IEEE) is a Senior Research Scientist working in the Artificial Intelligence Research Lab at Hewlett Packard Labs. Before joining Hewlett Packard Labs, he was a postdoctoral researcher at Politecnico di Milano (Italy). He worked across the stack of emerging in-memory computing accelerators, from nanoscale devices, novel analog circuits, microarchitecture, and HW/SW co-design. He has authored more than 40 papers and 4 book chapters. He is an IEEE Member. He received his Ph.D. (cum laude) in Electronics Engineering from Politecnico di Milano, Italy.

John Moon is a Post-doc in the emerging accelerator team at Hewlett Packard Labs, Milpitas (CA). He received his Ph.D. degree in 2021 from University of Michigan, Ann Arbor, MI, USA. His research includes designing an in-memory computing accelerator, simulating architectures, and applying it to AI/ML.

Pedro Bruel is a Research Scientist at Hewlett Packard Enterprise Labs. He received his PhD in Computer Science in 2021 at the University of Grenoble Alpes, France. His research interests are Statistical Learning and Optimal Experimental Design, applied to High Performance Computing domains such as hardware/software co-design, compiler optimization, and parallel and distributed computing.

Sergey Serebryakov Sergey is a machine learning engineer at Hewlett Packard Labs. He has worked on several projects including event and relation extraction from texts; benchmarking tools and performance analysis for deep learning workloads; and real-time anomaly detection for time series data. Currently, he focuses on research problems associated with collecting machine learning metadata and using it to accelerate machine learning pipelines, in particular, accelerating hyperparameter search with warmstarting and designing better hyperparameter search spaces. Sergey also serves as a co-chair of Best Practices working group in MLCommons organization that promotes industry-recognized deep learning benchmarks. Sergey got his Ph.D. from Saint-Petersburg Institute of Informatics and Automation, Master’s and Bachelor’s degrees from Saint-Petersburg State Polytechnical University.

Ron M. Roth (Fellow, IEEE) received the B.Sc. degree in computer engineering (1980), the M.Sc. in electrical engineering (1984), and the D.Sc. in computer science (1988) from Technion, Haifa, Israel. Since 1988 he has been with the CS Department at Technion, where he holds the General Yaakov Dori Chair in Engineering. During 1989–91 he was a Visiting Scientist at IBM, San Jose, CA, and during 1996–97, 2004–05, and 2011–12 he was on sabbatical leave at HP, Palo Alto, CA, and in 2022 at Hewlett Packard Enterprise, Milpitas, CA. Dr. Roth is the author of the book *Introduction to Coding Theory* (2006). His 1993 paper “New Array Codes for Multiple Phased Burst Correction,” co-authored with M. Blaum, received the 2021 *NVMW Persistent Impact Prize for ECC*. His research interests include coding theory, information theory, and their application to storage, computation, and the theory of complexity.

Luca Buonanno received a B.Sc. in Biomedical Engineering from Università degli studi di Napoli Federico II, an M.Sc. in Electronics Engineering from Politecnico di Milano, and a Ph.D. degree *cum laude* in Information Technology from Politecnico di Milano. He is now a researcher in HP Labs, investigating novel computing architectures and technologies for accelerating AI workloads.

Archit Gajjar received his Ph.D. in Computer Engineering from North Carolina State University. He worked as a Machine Learning Summer Intern at Hewlett Packard Enterprise in 2020-2022. He graduated with an M.S. in Computer Engineering from the University of Houston - Clear Lake. He received his B.Tech. from Dhirubhai Ambani Institute of Information and Communication Technology in India. Currently, he is a postdoctoral research associate in the Artificial Intelligence Research Lab at Hewlett Packard Labs. His research interests include applied AI/ML on customized hardware, FPGA hardware accelerators, and high-level synthesis hardware design.

Tobias Ziegler obtained his B. Sc. and M. Sc. degrees in Physics from RWTH Aachen University, Aachen, Germany in 2015 and 2018, respectively. He then pursued a Ph.D. degree in electrical engineering at the same university. For his contribution to the International Conference on Memristive Materials, Devices and Systems (Memrisys 2021) he was recognized with the excellent poster presentation award.

Cong Xu is currently a research scientist at Hewlett Packard Labs. His research interests include deep learning acceleration, high-performance computing, and distributed file systems. He has published more than 30 papers on non-volatile memory and deep learning acceleration. He co-lead the development of NVSim, which is a widely used simulation framework for non-volatile memories. Cong received his B.S. degree in microelectronics from Peking University, Beijing, in 2009, and his Ph.D. degree in computer science and engineering from Pennsylvania State University in 2015.

Martin Foltin is a principal research engineer at Hewlett Packard Labs in Fort Collins, Colorado. He has been with Hewlett Packard Enterprise (HPE) and Hewlett Packard (HP) for over 24 years in various roles spanning Silicon Design Automation, VLSI chip architecture and Artificial Intelligence. Martin currently manages the Data Foundation for AI engineering team at HPE AI Research Lab. Prior to this role he led the development of VLSI physical design automation workflows, VLSI and FPGA architectures for nonvolatile memory storage controllers, memristor-based inferencing AI accelerators, and industrial IoT controllers. Martin has PhD in Physics and Ms. in Physical Electronics, Optics and Plasma Physics. Prior to joining HPE, he served as Post-doctoral Fellow at the Pennsylvania State University and Colorado State University. During 30+ years of his professional career, Martin co-authored more than 20 US Patents and 40 publications in peer-reviewed journals and conferences.

Paolo Faraboschi (Fellow, IEEE) Paolo Faraboschi is a Vice President and HPE Fellow and directs the Artificial Intelligence Research Lab at Hewlett Packard Labs. Paolo worked on a broad range of technologies, from embedded printer processors, to exascale supercomputers. He previously led exascale computing research (2017-2020) and the hardware architecture of "The Machine" project (2014-2016), pioneered low-energy servers with HP's project Moonshot (2010-2014), drove scalable system-level simulation research (2004-2009), and was the principal architect of a family of embedded VLIW cores (1994-2003), widely used in video SoCs and HP's printers. Paolo is an IEEE Fellow (2014) for "contributions to embedded processor architecture and system-on-chip technology", author of 60 granted patents, over 100 publications, and the book "Embedded Computing: a VLIW approach". He received a Ph.D. in EECS from the University of Genoa, Italy.

Jim Ignowski (Senior Member, IEEE) received an MSEE degree from Stanford University in 1988 and a BSEE degree from Rice University in 1984. He is currently a Principal Research Engineer at Hewlett Packard Laboratories, managing the Emerging Accelerators Team in the Artificial Intelligence Research Lab. His current research interests include analog circuits for in-memory computing, ReRAM-based mixed-signal circuits for analog computation, and architectures to utilize these circuits for the acceleration of artificial intelligence workloads, emphasizing explainability, and in adjacent application spaces.

Catherine E. Graves is a Principal Research Scientist at Hewlett Packard Labs developing analog and neuromorphic computational accelerators leveraging emerging devices such as resistive RAM (RRAM). Some of her previous work utilized multilevel analog RRAM devices to natively perform matrix multiplication within crossbars, accelerating a core computation of wide-ranging applications from neural networks to signal processing. Currently, she leads a research team exploring RRAM-based associative memory circuits for tree-based ML and finite automata processing for network security and genomics applications. She was awarded Silicon Valley Intellectual Property Law Association (SVIPLA) Inventor of the Year in 2021 for her co-invention of analog content addressable memories. Cat received her Ph.D. in Applied Physics from Stanford University studying ultrafast magnetism for future magnetic memory technologies while an NSF Graduate Research Fellow. She has published over 35 peer-reviewed papers, three book chapters, and has been awarded 14 US patents.